Magnetic short-range order in β-$Mn_{1-x}Co_x$

2009 J. Phys.: Condens. Matter 21 124216

(http://iopscience.iop.org/0953-8984/21/12/124216)

J. Phys.: Condens. Matter **21** (2009) 124216 (6pp) doi:10.1088/0953-8984/21/12/124216

Magnetic short-range order in β-$Mn_{1-x}Co_x$

J R Stewart[1] **and R Cywinski**[2]

[1] ISIS, Rutherford Appleton Laboratory, Harwell Science and Innovation Campus, Didcot OX11 0QX, UK
[2] School of Applied Sciences, University of Huddersfield, Queensgate, Huddersfield HD1 3DH, UK

E-mail: ross.stewart@stfc.ac.uk

Received 28 November 2008, in final form 7 January 2009
Published 25 February 2009
Online at stacks.iop.org/JPhysCM/21/124216

Abstract

We present a study of the magnetic ground state properties of β-Mn metal alloyed with Co, using neutron polarization analysis of the diffuse neutron scattering cross-section. We analyse the magnetic structure obtained using a reverse Monte Carlo procedure to extract the Mn–Mn spin correlations. The addition of Co leads to a static disordered magnetic structure with medium-range correlations. Our analysis of the spin correlations indicates that both 8c and 12d non-equivalent lattice sites present in the β-Mn structure contribute to the magnetic ground state, where previously it was thought that the 8c site was non-magnetic.

(Some figures in this article are in colour only in the electronic version)

1. Introduction

Mn metal is, perhaps, the most inscrutable of the 3d transition metal elements. Its neighbouring 3d elements in the periodic table all have very simple crystal structures; to the left, vanadium and chromium (both bcc); to the right, iron (bcc), cobalt (hcp) and nickel (fcc). The room temperature phase of manganese, α-Mn, has bcc symmetry but with a very large unit cell which contains 58 Mn atoms distributed over four non-equivalent crystallographic sites [1]. The higher temperature (>710 °C) β-Mn phase is simple cubic, but still with a large unit cell containing 20 Mn atoms on two non-equivalent sites [2]. At higher temperatures still, γ-Mn and δ-Mn have simple (fcc) and (bcc) structures, respectively. While α- and γ-Mn both display antiferromagnetic order at low temperatures (the γ-phase being stabilized at low temperatures by the addition of e.g. Cu [3] or Ni [4]) and the ground state of the δ-Mn structure being calculated to be antiferromagnetic [5], the β-phase of elemental manganese (which is stable at low temperatures on rapid quenching) alone among the four manganese allotropes does not display long-range magnetic order down to the lowest temperatures studied. It is believed that there are two reasons for this; firstly, the β-phase of Mn is the closest packed of all the Mn structures, hampering moment formation on the Mn sites [6]; secondly, β-Mn is a geometrically frustrated system, with triangularly (or in some pictures, tetrahedrally) coordinated Mn atoms, unable to simultaneously satisfy antiferromagnetic bonds with each of their neighbours [7]. β-Mn does, however, display considerable short-range antiferromagnetic correlations of rapidly fluctuating Mn moments [8]. Taken together with the observation of a very large Sommerfeld constant, $\gamma \simeq 80$ mJ mol^{-1} K^{-2} [9], a $\sqrt{T}$ dependence of the NMR spin–lattice relaxation rate [10] and a $T^{\frac{3}{2}}$ dependence of electrical resistivity [8], self-consistent renormalization theory [11] suggests that β-Mn is a quantum-critical metal on the verge of antiferromagnetic order at $T = 0$, and a quantum-spin-liquid at higher temperatures. Intriguingly, the NMR and NQR measurements of Kohori and co-workers [10] suggest that large itinerant moments exist only on one of the two non-equivalent lattice sites, that being the 12d site (Mn2), which is a triangularly coordinated 'hyperkagome' lattice [12]. The 8c (Mn1) sites—which have a much smaller Mn–Mn near-neighbour distance—show a spin–lattice relaxation rate which is only 5% of that of the Mn2 sites, suggesting that the magnetism resides largely on the Mn2 sites.

Various studies of dilute β-Mn alloys with transition metals (such as Fe, Co) as well as non-transition metals (such as Al, Sn) have demonstrated that a small amount of impurity substitution is often sufficient to dampen the rapid spin fluctuations in β-Mn often resulting in a spin–glass like magnetic ground state at low temperatures. In the

case of Ru-, Ir- or Os- substitution, a long-range ordered incommensurate antiferromagnetic structure is stabilized at relatively high temperatures [13, 14]. There are three plausible mechanisms by which such a spin-liquid to static long-range or short-range order transition might proceed. Firstly, the substituent atoms may promote an expansion of the β-Mn lattice promoting the formation of localized magnetic moments on the Mn atoms. This appears to be the mechanism by which long-range order is produced in β-Mn alloys with Ru, Ir and Os, all of which display long-range order concomitant with a huge lattice expansion of around 5% by volume [15]. Secondly, the substituent atoms may donate holes or electrons to the conduction band, changing the density of electron/hole states at the Fermi energy, and resulting in sufficient exchange enhancement to promote static order (long- or short-range). This appears to be the mechanism for the formation of static but disordered ground states in β-Mn alloys with Fe [16] and Co [17]. Thirdly, the substituent atoms can disrupt the frustrated local topology of the Mn2 sites (or Mn1 and Mn2 sites), thereby lifting the spin-configurational degeneracy present in the frustrated lattice. This is thought to be important in the spin-liquid to spin–glass transition observed in β-$Mn_{1-x}Al_x$ alloys [12, 18, 19].

In this study, we concentrate on the β-$Mn_{1-x}Co_x$ system with Co concentrations of $x = 0.05$, 0.1 and 0.2. We will study the low temperature magnetic structure of these alloys using neutron diffraction with neutron polarization analysis to isolate the magnetic scattering function, and hence extract Mn–Mn correlations at low temperatures. We would, ideally, like to address the question of whether Mn moments exist on the Mn1 sites, since the evidence on this point is indirect (coming from NMR/NQR measurements). Additionally, *ab initio* DFT calculations of the magnetism on the β-Mn lattice suggest that there is indeed a sizeable magnetic moment associated with the Mn1 site [20].

2. Sample preparation and characterization

The β-$Mn_{1-x}Co_x$ samples used in this study were prepared by melting high-purity constituent metals in an argon arc-furnace. Each ingot was re-melted a number of times to ensure a homogeneous solid solution of Co in Mn. Each polycrystalline ingot was then annealed for 24 h in sealed quartz tubes under argon at 900 °C, and then rapidly quenched to room temperature by breaking the quartz tubes in water. That the samples were all in the β-phase was verified using x-ray diffraction. Further structural characterization of one of the samples (with Co concentration $x = 0.1$) was carried out using neutron diffraction. Figure 1 shows the room temperature diffraction pattern of β-$Mn_{0.9}Co_{0.1}$ taken using the LAD diffractometer at the ISIS pulsed neutron source, Didcot, UK. The data were modelled using the Rietveld refinement program GSAS [21], and indicate the β-phase with a lattice constant of 6.325(2) Å—roughly the same as that of pure β-Mn.

Due to the fact that Mn and Co have very different neutron scattering lengths ($b_{Mn} = -3.73 \times 10^{-15}$ m and $b_{Co} = +2.49 \times 10^{-15}$ m), the Bragg peak intensities are

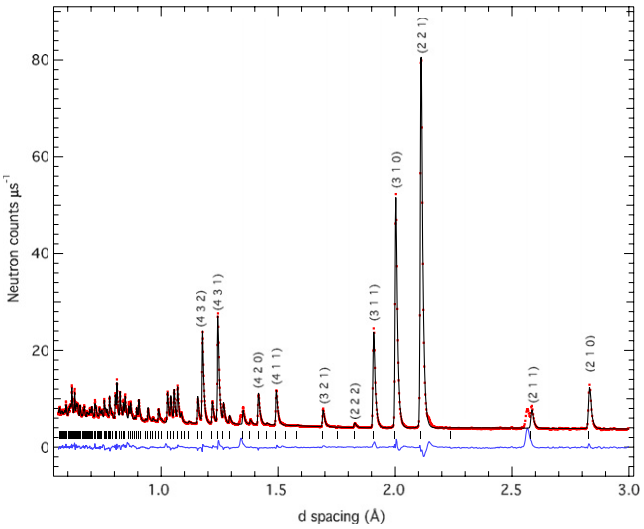

Figure 1. Room temperature neutron diffraction pattern of β-$Mn_{0.9}Co_{0.1}$ together with a Rietveld refinement fit and difference curve. The ticks indicate the positions of the β-Mn structural Bragg peaks, with the indices of the first few peaks shown. The impurity peaks at d spacings of ∼2.56 Å and ∼1.34 Å are, respectively, the (111) and (311) Bragg reflections from a small amount of MnO surface impurity.

sensitive to the site substitutional properties of Co in Mn. In the case of β-$Mn_{0.9}Co_{0.1}$ the Rietveld analysis reveals that the Co impurities reside solely on the Mn1 (8c) sublattice. The refined fractional occupancy of this site was 0.23(1), indicating a Co concentration of $x = 0.092$—very close to the nominal concentration of 0.1. This result confirms the earlier neutron diffraction study of Oyamatsu and co-workers [22]. Neutron diffraction spectra of β-$Mn_{1-x}Co_x$ with $x = 0.05$, 0.1 and 0.2 performed on the D1B spectrometer at the Institut Laue-Langevin (ILL), Grenoble, showed that the lattice constant does not vary with Co concentration across the entire concentration range. Magnetic characterization of the β-$Mn_{1-x}Co_x$ samples was carried out using an Oxford Instruments vibrating sample magnetometer (VSM). The dc magnetic susceptibility was determined by performing a field scan at constant temperature and then determining the gradient of the M–H line at zero-field. In this way, one may measure the susceptibility close to zero-field with high accuracy. Figure 2 shows the susceptibility of four β-$Mn_{1-x}Co_x$ alloys with $x = 0.05$, 0.1, 0.15 and 0.2. Each β-$Mn_{1-x}Co_x$ alloy displays a broad peak in the susceptibility increasing with temperature on increasing Co concentration from ∼20 K for $x = 0.05$ to ∼60 K for $x = 0.2$. The temperature independent susceptibility under the broad peak decreases with increasing Co concentration, indicating a possible reduction in the density of conduction electron states at the Fermi level. This would seem to indicate that β-$Mn_{1-x}Co_x$ is being pushed away from the critical boundary for spontaneous moment formation as Co is introduced into the β-Mn lattice. It should be stressed here that the susceptibility measurable using a standard VSM is the bulk, or $Q = 0$ susceptibility, and that it is likely that this represents only a small fraction of the total susceptibility which is known to be peaked at finite momentum transfer. For an

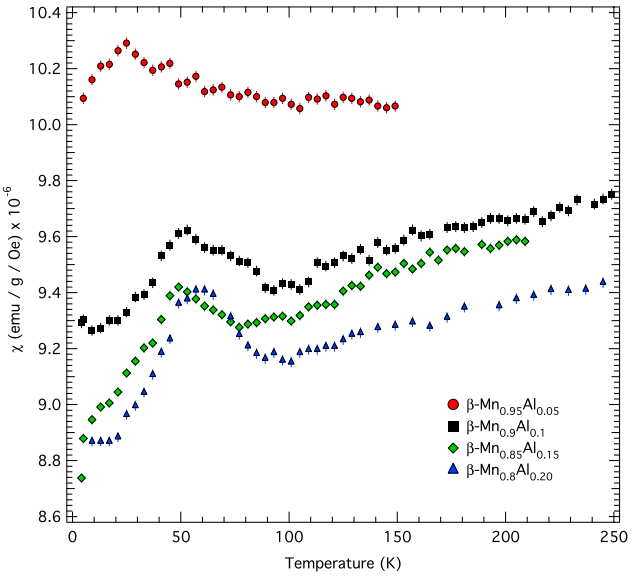

Figure 2. Magnetic susceptibility of β-$Mn_{1-x}Co_x$ alloys with $x = 0.05, 0.1, 0.15$ and 0.2.

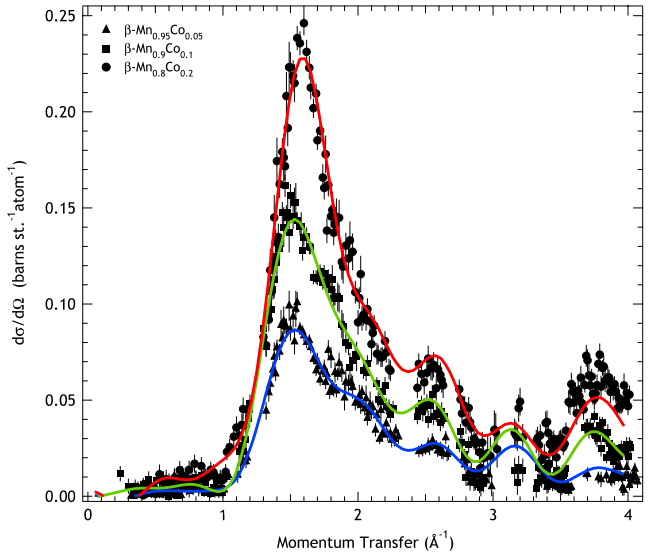

Figure 3. The magnetic scattering function $S(Q)$ measured using neutron polarization analysis, of β-$Mn_{1-x}Co_x$ with $x = 0.05, 0.1$ and 0.2. The cross-sections were all measured at low temperature, $T = 2$ K. The solid lines through the data are reverse Monte Carlo fits as described in the text.

itinerant antiferromagnet, the application of an external field need not necessarily induce a bulk magnetization as it would for a local moment antiferromagnet, so it is likely that the dc-susceptibility data presented here do not give a good indication of the magnetic properties of β-$Mn_{1-x}Co_x$.

3. Neutron polarization analysis diffraction

We have measured neutron diffraction spectra of β-$Mn_{1-x}Co_x$ with $x = 0.05$, 0.1 and 0.2 on the polarized neutron diffuse scattering spectrometer, D7 at the ILL [23]. Using 'xyz'-polarization analysis, we have been able to extract the magnetic scattering from the nuclear coherent and nuclear spin-incoherent scattering cross-sections [24]. Inspection of the nuclear structure factor reveals a flat diffuse background, indicating a random solid solution of Co on the Mn1 sublattice. The magnetic-only scattering cross-sections of β-$Mn_{1-x}Co_x$ alloys with $x = 0.05$, 0.1 and 0.2 are shown in figure 3. Each Co concentration displays a broad diffuse peak centred around a momentum transfer of $Q \simeq 1.5$ Å^{-1}, with smaller peaks at momentum transfers of around 2, 2.6, 3.2 and 3.8 Å^{-1}. The integrated intensity under the magnetic cross-sections increases dramatically on increasing Co concentration. This may indicate either an increasing Mn/Co moment, or it may be due to a dynamical effect, whereby the fluctuation rates of the Mn/Co spins slow down sufficiently to be covered by the frequency range of the neutron scattering instrument. On the D7 spectrometer, with an incident wavelength of $\lambda = 3.1$ Å, spin fluctuations of frequency less than 3.5 meV ($\equiv 8.5 \times 10^{11}$ Hz) will contribute to the magnetic scattering function. Higher frequency spin fluctuations will not be countable by the instrument.

To model the diffuse scattering data, we have employed a reverse Monte Carlo algorithm (RMC) used previously in our investigations of β-MnAl alloys [19]. We generate a large box (in this case $6 \times 6 \times 6$ β-Mn unit cells) of Mn/Co atoms, and assign a Heisenberg spin of equal and fixed magnitude and random orientation at each site. The spin–spin correlations, $\langle \vec{S}_0 \cdot \vec{S}_i \rangle$ for the ith near-neighbour shell are computed from the model and the magnetic scattering cross-section is then calculated via the standard expression for a magnetically disordered polycrystalline material,

$$\left(\frac{d\sigma}{d\Omega}\right)_{mag} = \frac{2}{3}\left(\frac{\gamma_n r_0}{2}\right)^2 f^2(\vec{Q}) g_S^2 S(S+1) \times \left[1 + \sum_i Z_i \frac{\langle \vec{S}_0 \cdot \vec{S}_i \rangle}{S(S+1)} \frac{\sin(Qr_i)}{Qr_i}\right]$$

where, the sum runs over i near-neighbour shells. γ_n is the neutron gyromagnetic ratio, r_0 is the classical electron radius, $r_0 = \mu_0 e^2/4\pi m_e$, $f(Q)$ is the magnetic form factor of the magnetic species used in the model (Mn^{3+} in this case), $g_s^2 S(S+1)$ is the squared magnetic moment of the magnetic species and Z_i and r_i are the co-ordination number and radial distance of the ith near-neighbour shell respectively. The computed cross-section is then compared with the data and a χ^2 value computed. After this initial step, the spins are randomly rotated one-by-one, and the cross-section recalculated. Spin rotations which reduce the value of χ^2 are accepted, while rotations which increase χ^2 are rejected.

In the case of β-$Mn_{1-x}Co_x$, we have tried two RMC models to fit the data. The first model assumes that magnetic moments reside only on the Mn2 sites—in agreement with NMR studies [10], and our own model for the β-MnAl system [19]. The second model makes no such assumption and equally assigns magnetic moments to both the Mn1 and Mn2 sublattices. A comparison of these two RMC model fits is shown in figure 4. The RMC model with both the Mn1 and Mn2 sublattices describes the data much better than the Mn2

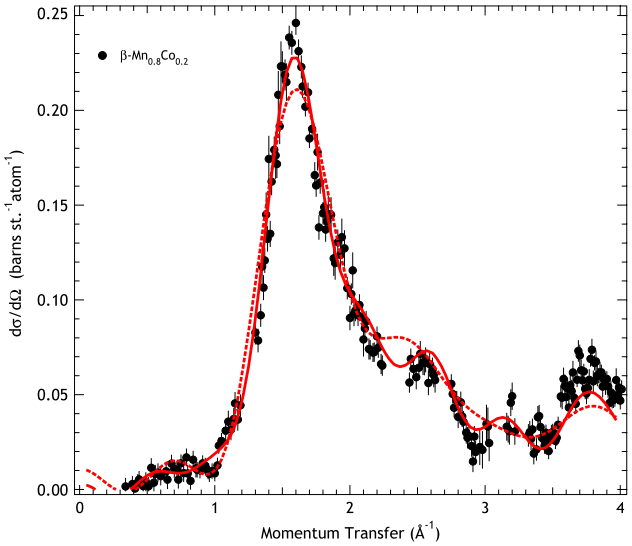

Figure 4. Comparison of the two RMC models attempted in order to fit the β-$Mn_{0.8}Al_{0.2}$ magnetic $S(Q)$. The dashed line represents the model with only the Mn2 sites contributing to the magnetic scattering. The solid line shows the RMC model with both Mn1 and Mn2 sublattices included.

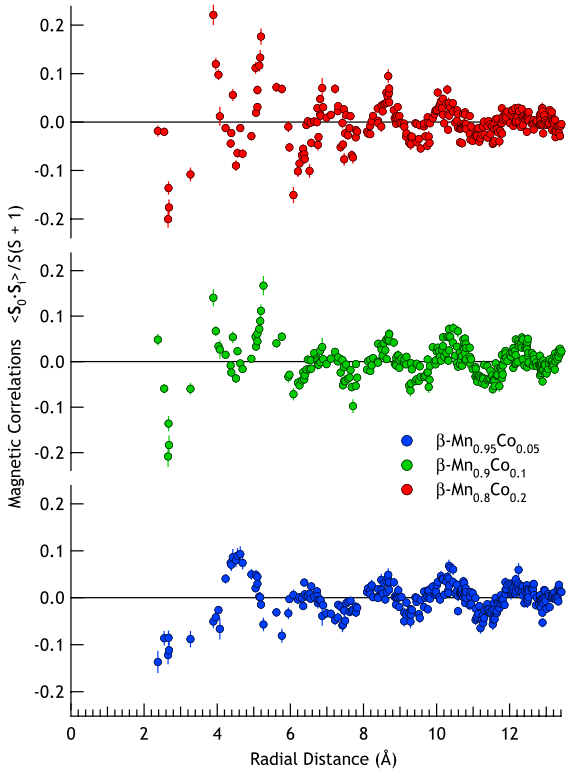

Figure 5. The magnetic correlations over the first 300 near-neighbour shells of β-$Mn_{1-x}Co_x$ with $x = 0.05$ (blue, lower), 0.1 (green, middle) and 0.2 (red, upper).

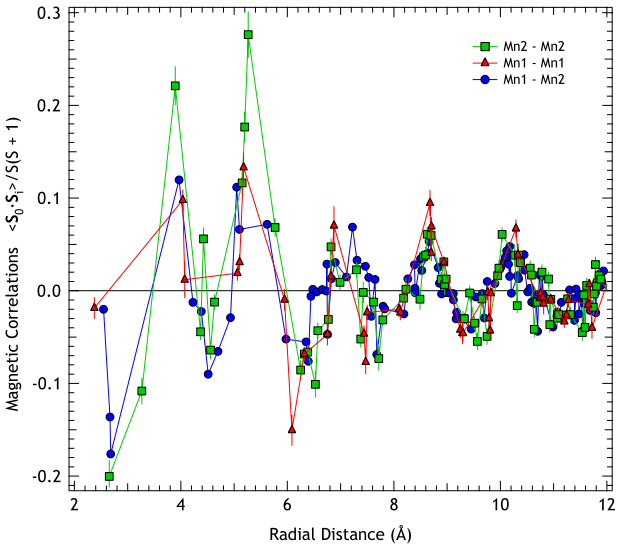

Figure 6. The magnetic correlations $\beta Mn_{0.8}Al_{0.2}$, with the Mn1–Mn1 (red, triangles), Mn2–Mn2 (green, squares) and Mn1–Mn2 (blue, circles) correlations shown separately.

only model, with values of $\chi^2 = 6.52$ for the Mn2 only model, and $\chi^2 = 3.08$ for the full-lattice model. The Mn2 model fails to reproduce the peaks in the data at 2.6 and 3.2 $Å^{-1}$, and does not reproduce the main peak at 1.5 $Å^{-1}$ well. The mean magnetic moments extracted from the RMC fits were 1.12(1) μ_B for β-$Mn_{0.95}Co_{0.05}$, 1.41(1) μ_B for β-$Mn_{0.9}Co_{0.1}$ and 1.71(1) μ_B for β-$Mn_{0.8}Co_{0.2}$. It should be emphasized here that these moments are the average moments per Mn/Co atom, for spins fluctuating within the frequency window of D7.

The magnetic correlations extracted from the full-lattice model for each of the β-$Mn_{1-x}Co_x$ compositions is shown in figure 5. The correlations are oscillatory indicating predominantly antiferromagnetic exchange between the Mn/Co atoms. They are also of a considerable range, with oscillations still visible out to a radial correlation distance of 13.5 Å (corresponding to the first 300 near-neighbour shells in the β-Mn lattice). The $x = 0.05$ concentration shows a strong peak in the correlations at around 4.5 Å, which goes over to two large peaks at 3.8 and 5.2 Å for the $x = 0.1$ and 0.2 concentrations. Figure 6 shows the near-neighbour correlations of the β-$Mn_{0.8}Al_{0.2}$ composition, with each of the partial correlations (Mn1–Mn1, Mn2–Mn2 and Mn1–Mn2) shown separately. We note that the strongest correlations, $\langle \vec{S}_0 \cdot \vec{S}_4 \rangle = -0.2$ at ~2.6 Å and $\langle \vec{S}_0 \cdot \vec{S}_7 \rangle = +0.22$ at ~3.8 Å and $\langle \vec{S}_0 \cdot \vec{S}_{27} \rangle = +0.28$ at ~5.2 Å are all Mn2–Mn2 correlations indicating that the Mn2 site is the more strongly correlated of the two sites. It is however clear that the Mn1 and Mn1–Mn2 correlations—especially at larger distances—are just as strong as the Mn2 correlations.

4. Discussion

The assignment of a magnetic moment to the Mn1 β-Mn sublattice runs contrary to much of the published literature on β-Mn. Only in the antiferromagnetically ordered β-MnRu alloys is there any evidence for the existence of a magnetic moment on the Mn1 sites [14]—and in that case, Rietveld analysis of the magnetic long-range ordered ground state is unable to distinguish between models where there are moments on both β-Mn sublattices, or just the Mn2 sublattice. For β-

MnRu, the Ru atoms preferentially occupy the Mn1 sublattice, as the Co do in this study, however, Ru doping also introduces a truly massive volume expansion in the β-Mn lattice, which the Co does not. Our data do seem to indicate that the Mn1 sublattice does participate in the magnetic structure of, at the least, the β-$Mn_{1-x}Co_x$ alloys studied here. However, there are some shortcomings with the model we use. Chief among these is the assumption of equal magnetic moments on the Mn1 and Mn2 sites, as well as on the Mn and Co atoms. This assumption is necessary in order to extract meaningful magnetic correlations from polycrystalline data. Further information on the separate sublattice moments of Mn1 and Mn2 as well as the impurity moment on the Co site would be readily extracted from single crystals of β-MnCo, and efforts are currently underway to produce these.

In support of our findings, various DFT band-structure calculations of β-Mn have been carried out which do not agree with the picture of a non-magnetic Mn1 sublattice [20, 25]. Instead they predict ferrimagnetic order between *ferromagnetically* correlated Mn1 and Mn2 sublattices. This suggests that the dominant interaction in β-Mn is an antiferromagnetic Mn1–Mn2 interaction, rather than the antiferromagnetic Mn2–Mn2 interaction normally assumed. Another possible model, called 'nearly least frustrated antiferromagnetic' has been put forward by Asada [26], in which collinear ferromagnetic order on the Mn1 lattice coexists with a disordered Mn2 sublattice. None of these models particularly correspond with our observations (although from figure 5, there is a tantalizing indication of a weak ferromagnetic Mn1–Mn1 1st near-neighbour correlation in the β-$Mn_{0.9}Al_{0.1}$ composition) but it is noticeable that band-structure calculations of the Mn1 sublattice all predict some sort of magnetic moment associated with that site, albeit smaller in magnitude than the Mn2 moment.

5. Conclusions

We have characterized the static magnetic ground state of β-$Mn_{1-x}Co_x$ alloys using neutron polarization analysis. Neutron diffraction shows that the Co substituent atom solely occupy the closer packed 8c (Mn1) site. The diffuse magnetic scattering cross-section at low temperatures, has been described using a model of equal disordered moments on both the 8c (Mn1) and 12d (Mn2) crystallographic sites. This result calls into question the conventional wisdom of the magnetic properties of β-Mn which assert that significant magnetic moments exist only in the Mn2 site.

Acknowledgments

The authors would like to thank the technical support staff at the ILL and ISIS for their invaluable help during these experiments. In particular we thank D A Keen (ISIS) for scientific support, and B D Rainford for scientific discussions.

References

[1] Bradley A J and Thewlis J 1927 The crystal structure of α-manganese *Proc. R. Soc.* A **115** 456–71
[2] Shoemaker C B, Shoemaker D P, Hopkins T E and Yindepit S 1978 Refinement of the structure of β-manganese and of a related phase in the Mn–Ni–Si system *Acta Crystallogr.* B **34** 3573–6
[3] Cowlam N and Shamah A M 1981 A diffraction study of γ-MnCu alloys *J. Phys. F: Met. Phys.* **11** 27–43
[4] Long M W and Moze O 1990 Magnetic diffuse scattering and the triple-q structure in FCC γ-MnNi *J. Phys.: Condens. Matter* **2** 6013–30
[5] Kübler J 1980 Calculated magnetic moment of δ-manganese *J. Magn. Magn. Mater.* **20** 107–10
[6] Stewart J R and Cywinski R 1999 Real-time kinetic neutron powder diffraction study of the α-Mn to β-Mn phase transition *J. Phys.: Condens. Matter* **11** 7095–102
[7] Canals B and Lacroix C 2000 Mean-field study of the disordered ground state in the β-Mn lattice *Phys. Rev.* B **61** 11251–4
[8] Stewart J R, Rainford B D, Eccleston R S and Cywinski R 2002 Non-Fermi-liquid behavior of electron-spin fluctuations in an elemental paramagnet *Phys. Rev. Lett.* **89** 186403
[9] Shinkoda T, Kumagai K and Asayama K 1979 Effect of spin-fluctuations on the specific heat in β-Mn metal and alloys *J. Phys. Soc. Japan* **46** 1754–8
[10] Kohori Y, Noguchi Y and Kohara T 1993 Observation of ^{55}Mn NMR and NQR signals from site II in β-Mn metal *J. Phys. Soc. Japan* **62** 447–50
[11] Moriya T 1985 *Spin Fluctuations in Itinerant Electron Magnetism* (Berlin: Springer)
[12] Nakamura H, Yoshimoto K, Shiga M, Nishi M and Kakurai K 1997 Strong antiferromagnetic spin fluctuations and the quantum spin liquid state in geometrically frustrated β-Mn, and the transition to a spin-glass state caused by non-magnetic impurity *J. Phys.: Condens. Matter* **9** 4701–28
[13] Miyakawa M, Umetsu R Y, Ohta M, Fujita A, Fukamichi K and Hori T 2005 Spin fluctuation, thermal expansion anomaly, and pressure effects on the Néel temperature of β-MnM (M = Ru, Os, and Ir) alloys *Phys. Rev.* B **72** 054420
[14] Stewart J R, Wills A S, Leavey C J, Rainford B D and Ritter C 2007 The magnetic structure of β-MnRu *J. Phys.: Condens. Matter* **19** 145291
[15] Miyakawa M, Umetsu R Y, Sasao K and Fukamichi K 2003 Antiferromagnetism and low-temperature specific heat of β-$Mn_{1-x}Ir_x$ alloys *J. Phys.: Condens. Matter* **15** 4605–12
[16] Nishihara Y, Ogawa S and Waki S 1977 Mössbauer study of β-Mn alloys with iron and tin—weak itinerant electron antiferromagnetism of β-Mn alloys *J. Phys. Soc. Japan* **42** 845–52
[17] Funahashi S and Kohara T 1984 Neutron diffuse scattering in β-Mn *J. Appl. Phys.* **55** 2048–50
[18] Stewart J R and Cywinski R 1999 μSR evidence for the spin-liquid to spin-glass transition in β-$Mn_{1-x}Al_x$ *Phys. Rev.* B **59** 4305–13
[19] Stewart J R, Andersen K H and Cywinski R 2008 Neutron polarization analysis study of the frustrated magnetic ground state of β-$Mn_{1-x}Al_x$ *Phys. Rev.* B **78** 014428
[20] Hafner J and Hobbs D 2003 Understanding the complex metallic element Mn. II. Geometric frustration in β-Mn, phase stability, and phase transitions *Phys. Rev.* B **68** 014408
[21] Larson A C and Von Dreele R B 1994 GSAS: general structure analysis system *Technical Report* LAUR-86-748, Los Alamos National Laboratory
[22] Oyamatsu H, Nakai Y and Kunitomi N 1989 Impurity distribution on the sites of β-Mn structure for Mn(Co), Mn(Fe) and Mn(Ni) alloys *J. Phys. Soc. Japan* **58** 3606–15
[23] Stewart J R, Andersen K H, Cywinski R and Murani A P 2000 Magnetic diffuse scattering in disordered systems studied by neutron polarization analysis *J. Appl. Phys.* **87** 5425–9

[24] Schärpf O and Capellmann H 1993 The XYZ-difference method with polarized neutrons and the separation of coherent, spin incoherent and magnetic scattering cross sections in a multidetector *Phys. Status Solidi* a **135** 359–79

[25] Sliwko V, Hohn P and Schwarz K 1994 The electronic and magnetic structures of α- and β-manganese *J. Phys.: Condens. Matter* **6** 6557–64

[26] Asada T 1995 Electronic structures and magnetism of α and β Mn *J. Magn. Magn. Mater.* **140–144** 47–8